Editors' Suggestion

Direct Measurement of the Cosmic-Ray Proton Spectrum from 50 GeV to 10 TeV with the Calorimetric Electron Telescope on the International Space Station

O. Adriani,[1,2] Y. Akaike,[3,4] K. Asano,[5] Y. Asaoka,[6,7,*] M. G. Bagliesi,[8,9] E. Berti,[1,2] G. Bigongiari,[8,9] W. R. Binns,[10] S. Bonechi,[8,9] M. Bongi,[1,2] P. Brogi,[8,9] A. Bruno,[11] J. H. Buckley,[10] N. Cannady,[12] G. Castellini,[13] C. Checchia,[14,15] M. L. Cherry,[12] G. Collazuol,[14,15] V. Di Felice,[16,17] K. Ebisawa,[18] H. Fuke,[18] T. G. Guzik,[12] T. Hams,[3,19] N. Hasebe,[6] K. Hibino,[20] M. Ichimura,[21] K. Ioka,[22] W. Ishizaki,[5] M. H. Israel,[10] K. Kasahara,[6] J. Kataoka,[6] R. Kataoka,[23] Y. Katayose,[24] C. Kato,[25] N. Kawanaka,[26,27] Y. Kawakubo,[12,28] K. Kohri,[29] H. S. Krawczynski,[10] J. F. Krizmanic,[19,3] T. Lomtadze,[9] P. Maestro,[8,9] P. S. Marrocchesi,[8,9,†] A. M. Messineo,[30,9] J. W. Mitchell,[4] S. Miyake,[31] A. A. Moiseev,[32,19] K. Mori,[6,18] M. Mori,[33] N. Mori,[2] H. M. Motz,[34] K. Munakata,[25] H. Murakami,[6] S. Nakahira,[35] J. Nishimura,[18] G. A. de Nolfo,[11] S. Okuno,[20] J. F. Ormes,[36] S. Ozawa,[6] L. Pacini,[1,13,2] F. Palma,[16,17] P. Papini,[2] A. V. Penacchioni,[8,37] B. F. Rauch,[10] S. B. Ricciarini,[13,2] K. Sakai,[19,3] T. Sakamoto,[28] M. Sasaki,[19,32] Y. Shimizu,[20] A. Shiomi,[38] R. Sparvoli,[16,17] P. Spillantini,[1] F. Stolzi,[8,9] J. E. Suh,[8,9] A. Sulaj,[8,9] I. Takahashi,[39] M. Takayanagi,[18] M. Takita,[5] T. Tamura,[20] T. Terasawa,[35] H. Tomida,[18] S. Torii,[6,40,‡] Y. Tsunesada,[41] Y. Uchihori,[42] S. Ueno,[18] E. Vannuccini,[2] J. P. Wefel,[12] K. Yamaoka,[43] S. Yanagita,[44] A. Yoshida,[28] and K. Yoshida[45]

(CALET Collaboration)

[1]*Department of Physics, University of Florence, Via Sansone, 1—50019 Sesto, Fiorentino, Italy*
[2]*INFN Sezione di Florence, Via Sansone, 1—50019 Sesto, Fiorentino, Italy*
[3]*Department of Physics, University of Maryland, Baltimore County, 1000 Hilltop Circle, Baltimore, Maryland 21250, USA*
[4]*Astroparticle Physics Laboratory, NASA/GSFC, Greenbelt, Maryland 20771, USA*
[5]*Institute for Cosmic Ray Research, The University of Tokyo, 5-1-5 Kashiwa-no-Ha, Kashiwa, Chiba 277-8582, Japan*
[6]*Waseda Research Institute for Science and Engineering, Waseda University, 3-4-1 Okubo, Shinjuku, Tokyo 169-8555, Japan*
[7]*JEM Utilization Center, Human Spaceflight Technology Directorate, Japan Aerospace Exploration Agency, 2-1-1 Sengen, Tsukuba, Ibaraki 305-8505, Japan*
[8]*Department of Physical Sciences, Earth and Environment, University of Siena, via Roma 56, 53100 Siena, Italy*
[9]*INFN Sezione di Pisa, Polo Fibonacci, Largo B. Pontecorvo, 3—56127 Pisa, Italy*
[10]*Department of Physics and McDonnell Center for the Space Sciences, Washington University, One Brookings Drive, St. Louis, Missouri 63130-4899, USA*
[11]*Heliospheric Physics Laboratory, NASA/GSFC, Greenbelt, Maryland 20771, USA*
[12]*Department of Physics and Astronomy, Louisiana State University, 202 Nicholson Hall, Baton Rouge, Louisiana 70803, USA*
[13]*Institute of Applied Physics (IFAC), National Research Council (CNR), Via Madonna del Piano, 10, 50019 Sesto, Fiorentino, Italy*
[14]*Department of Physics and Astronomy, University of Padova, Via Marzolo, 8, 35131 Padova, Italy*
[15]*INFN Sezione di Padova, Via Marzolo, 8, 35131 Padova, Italy*
[16]*University of Rome "Tor Vergata", Via della Ricerca Scientifica 1, 00133 Rome, Italy*
[17]*INFN Sezione di Rome "Tor Vergata", Via della Ricerca Scientifica 1, 00133 Rome, Italy*
[18]*Institute of Space and Astronautical Science, Japan Aerospace Exploration Agency, 3-1-1 Yoshinodai, Chuo, Sagamihara, Kanagawa 252-5210, Japan*
[19]*CRESST and Astroparticle Physics Laboratory NASA/GSFC, Greenbelt, Maryland 20771, USA*
[20]*Kanagawa University, 3-27-1 Rokkakubashi, Kanagawa, Yokohama, Kanagawa 221-8686, Japan*
[21]*Faculty of Science and Technology, Graduate School of Science and Technology, Hirosaki University, 3, Bunkyo, Hirosaki, Aomori 036-8561, Japan*
[22]*Yukawa Institute for Theoretical Physics, Kyoto University, Kitashirakawa Oiwakecho, Sakyo, Kyoto 606-8502, Japan*
[23]*National Institute of Polar Research, 10-3, Midori-cho, Tachikawa, Tokyo 190-8518, Japan*
[24]*Faculty of Engineering, Division of Intelligent Systems Engineering, Yokohama National University, 79-5 Tokiwadai, Hodogaya, Yokohama 240-8501, Japan*
[25]*Faculty of Science, Shinshu University, 3-1-1 Asahi, Matsumoto, Nagano 390-8621, Japan*
[26]*Hakubi Center, Kyoto University, Yoshida Honmachi, Sakyo-ku, Kyoto 606-8501, Japan*
[27]*Department of Astronomy, Graduate School of Science, Kyoto University, Kitashirakawa Oiwake-cho, Sakyo-ku, Kyoto 606-8502, Japan*
[28]*College of Science and Engineering, Department of Physics and Mathematics, Aoyama Gakuin University, 5-10-1 Fuchinobe, Chuo, Sagamihara, Kanagawa 252-5258, Japan*
[29]*Institute of Particle and Nuclear Studies, High Energy Accelerator Research Organization, 1-1 Oho, Tsukuba, Ibaraki 305-0801, Japan*

[30]University of Pisa, Polo Fibonacci, Largo B. Pontecorvo, 3—56127 Pisa, Italy
[31]Department of Electrical and Electronic Systems Engineering, National Institute of Technology, Ibaraki College, 866 Nakane, Hitachinaka, Ibaraki 312-8508 Japan
[32]Department of Astronomy, University of Maryland, College Park, Maryland 20742, USA
[33]Department of Physical Sciences, College of Science and Engineering, Ritsumeikan University, Shiga 525-8577, Japan
[34]Faculty of Science and Engineering, Global Center for Science and Engineering, Waseda University, 3-4-1 Okubo, Shinjuku, Tokyo 169-8555, Japan
[35]RIKEN, 2-1 Hirosawa, Wako, Saitama 351-0198, Japan
[36]Department of Physics and Astronomy, University of Denver, Physics Building, Room 211, 2112 East Wesley Avenue, Denver, Colorado 80208-6900, USA
[37]ASI Science Data Center (ASDC), Via del Politecnico snc, 00133 Rome, Italy
[38]College of Industrial Technology, Nihon University, 1-2-1 Izumi, Narashino, Chiba 275-8575, Japan
[39]Kavli Institute for the Physics and Mathematics of the Universe, The University of Tokyo, 5-1-5 Kashiwanoha, Kashiwa, 277-8583, Japan
[40]School of Advanced Science and Engineering, Waseda University, 3-4-1 Okubo, Shinjuku, Tokyo 169-8555, Japan
[41]Division of Mathematics and Physics, Graduate School of Science, Osaka City University, 3-3-138 Sugimoto, Sumiyoshi, Osaka 558-8585, Japan
[42]National Institutes for Quantum and Radiation Science and Technology, 4-9-1 Anagawa, Inage, Chiba 263-8555, Japan
[43]Nagoya University, Furo, Chikusa, Nagoya 464-8601, Japan
[44]College of Science, Ibaraki University, 2-1-1 Bunkyo, Mito, Ibaraki 310-8512, Japan
[45]Department of Electronic Information Systems, Shibaura Institute of Technology, 307 Fukasaku, Minuma, Saitama 337-8570, Japan

(Received 28 December 2018; revised manuscript received 3 March 2019; published 10 May 2019)

In this paper, we present the analysis and results of a direct measurement of the cosmic-ray proton spectrum with the CALET instrument onboard the International Space Station, including the detailed assessment of systematic uncertainties. The observation period used in this analysis is from October 13, 2015 to August 31, 2018 (1054 days). We have achieved the very wide energy range necessary to carry out measurements of the spectrum from 50 GeV to 10 TeV covering, for the first time in space, with a single instrument the whole energy interval previously investigated in most cases in separate subranges by magnetic spectrometers (BESS-TeV, PAMELA, and AMS-02) and calorimetric instruments (ATIC, CREAM, and NUCLEON). The observed spectrum is consistent with AMS-02 but extends to nearly an order of magnitude higher energy, showing a very smooth transition of the power-law spectral index from -2.81 ± 0.03 (50–500 GeV) neglecting solar modulation effects (or -2.87 ± 0.06 including solar modulation effects in the lower energy region) to -2.56 ± 0.04 (1–10 TeV), thereby confirming the existence of spectral hardening and providing evidence of a deviation from a single power law by more than 3σ.

DOI: 10.1103/PhysRevLett.122.181102

Introduction.—Direct measurements of the high-energy (HE) spectra of each species of cosmic-ray nuclei up to the PeV energy scale provide detailed insight into the general phenomenology of cosmic-ray acceleration and propagation in the Galaxy. A possible charge-dependent cutoff in the nuclei spectra is hypothesized to explain the "knee" in the all-particle spectrum. This hypothesis can be tested directly with measurements by long duration space experiments with sufficient exposure and with the capability of identifying individual elements based on charge measurements.

Furthermore, the spectral hardening observed in the spectra of various nuclei [1–11] calls for the extensive attempts [12–32] to theoretically interpret these unexpected phenomena. The current experimental approaches to direct measurements of the proton spectrum are based on two main classes of instruments, i.e., magnetic spectrometers [5,6] at lower energies where the presence of a spectral breakpoint was observed, and calorimeters [1,4,8,33,34] at higher energies where the spectrum undergoes a hardening. It is of particular interest to determine the onset of spectral hardening and its development in terms of index variation and smoothness parameter (as defined in Ref. [6]). In order to achieve a consistent picture, measurements should be unaffected, as much as possible, by systematic errors and a critical comparison of the observations from different experiments is in order.

The CALorimetric Electron Telescope (CALET) [35,36], a space-based instrument optimized for the measurement of the all-electron spectrum [37,38] and equipped with a fully active calorimeter, can measure the main components of cosmic rays including proton, light, and heavy nuclei (up to iron and above) in the energy range up to ~1 PeV. The thickness of the calorimeter corresponds to 30 radiation length (at normal incidence) and to ~1.3 proton interaction length.

In this Letter, we present a direct measurement of the cosmic-ray proton spectrum from $E = 50$ GeV to 10 TeV with CALET where E denotes the kinetic energy of primary protons throughout this paper. Its wide dynamic range allows the study of the detailed shape of the spectrum by using a single instrument.

CALET Instrument.—CALET consists of a charge detector (CHD), a 3 radiation-length thick imaging calorimeter (IMC) and a 27 radiation-length thick total absorption calorimeter (TASC), with a field of view of ~45° from zenith. A "fiducial" geometrical factor of ~416 cm^2 sr for particles penetrating CHD top to TASC bottom, with 2 cm margins at the first and the last TASC layers (acceptance A), and corresponding to about 40% of the total acceptance [38], is used in this analysis.

The CHD, which identifies the charge of the incident particle, is comprised of a pair of plastic scintillator hodoscopes arranged in two orthogonal layers. The IMC is a sampling calorimeter alternating thin layers of Tungsten absorber with layers of scintillating fibers readout individually, also providing an independent charge measurement via multiple dE/dx samples. The TASC is a tightly packed lead-tungstate ($PbWO_4$) hodoscope, measuring the energy of showering particles in the detector. A very large dynamic range of more than 6 orders of magnitude is covered by four different gain ranges [39]. A more complete description of the instrument is given in the Supplemental Material of Ref. [37].

Figure 1 shows a proton candidate with energy deposit of ~10 TeV in the detector. The event example clearly demonstrates CALET's capability to reconstruct and identify very high energy protons. Because of the limited energy resolution, energy unfolding is required to estimate the primary energy distribution. It is important, therefore, to infer the detector response at the highest energies covered by the analysis.

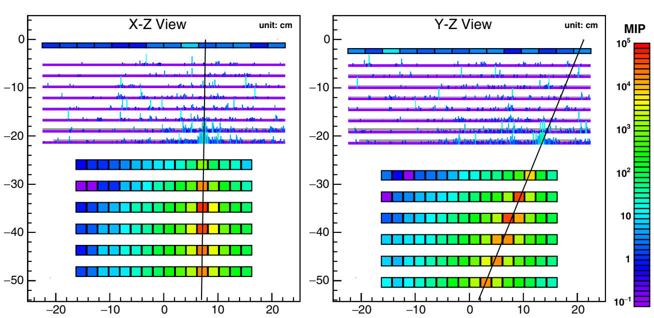

FIG. 1. An example of a high-energy proton event with an energy deposit sum of 10 TeV. Black lines represent the reconstructed tracks using Kalman filter tracking [40], which achieves a fine resolution taking advantage of the high granularity of the IMC.

The instrument was launched on August 19, 2015 and emplaced on the Japanese Experiment Module-Exposed Facility on the International Space Station with an expected mission duration of five years (or more). Scientific observations [36] started on October 13, 2015, and smooth and continuous operations have taken place since then.

Data analysis.—We have analyzed flight data collected for 1054 days from October 13, 2015 to August 31, 2018. The total observation live time for the HE shower trigger [36] is 21421.9 hours and live time fraction to total time is 84.7%. In addition, the low-energy (LE) shower trigger operated at a high geomagnetic latitude [36] is used to extend the energy coverage toward the lower energy region. In spite of a limited live time of 365.4 hr, LE data provide sufficient statistics for protons below a few hundred GeV.

Monte Carlo (MC) simulations, reproducing the detailed detector configuration, physics processes, as well as detector signals, are based on the EPICS simulation package [41,42].

In order to assess the relatively large uncertainties in the hadronic interactions, a series of beam tests were carried out at CERN-SPS using the CALET beam test model [43–45]. Trigger efficiency and energy response derived from MC simulations were tuned using the beam test results obtained in 2012 [43,44,46] with proton beams of 30, 100, and 400 GeV. The correction for the trigger efficiency obtained by the EPICS simulation was determined to be 7.7% for the LE trigger and 11.2% for the HE trigger, irrespective of proton energies. Shower energy correction was determined to be 7.9% and 6.3% at 30 and 100 GeV, and no correction at 400 GeV and above, where simple log-linear interpolation was used to determine the correction factor for intermediate energies.

In the analysis of hadrons, especially in the high-energy region where no beam test calibration is possible, a comparison between different MC models becomes much more important than in electron analysis. For this purpose, we have run simulations with FLUKA [47–49] and GEANT4 [50,51] in the same way as EPICS. The detector models used in FLUKA and GEANT4 are almost identical to the CALET CAD model used in EPICS.

In electron analysis [37,38], the electromagnetic shower tracking algorithm works very well, because of the presence of a developed shower core that is used as an initial guess of the trajectory of the incoming particle. In the proton analysis, however, the hadronic interaction occurs abruptly and there is no guarantee of the presence of a well-developed shower core in the bottom two layers of the IMC. It is therefore necessary to follow a different approach to reconstruct the proton tracks in a highly efficient way. Combinatorial Kalman filter tracking [40] was developed for this purpose and it is used in the proton spectrum analysis described hereafter.

The shower energy of each event is calculated as the TASC energy deposit sum (observed energy: E_{TASC}), which is calibrated using penetrating particles and by performing a seamless stitching of adjacent gain ranges on orbit, complemented by the confirmation of the linearity of the system over the whole range by means of ground measurements using UV pulse laser as described in Ref. [39]. Temporal variations during the long-term observation are also corrected, sensor by sensor, using penetrating particles as gain monitor [37].

In order to minimize helium contamination by accurately separating protons from helium based on their charge, a preselection of well-reconstructed and well-contained events is applied. Preselection consists of (1) offline trigger confirmation, (2) geometrical condition (requires acceptance A [38]), (3) track quality cut to ensure reliability of the reconstructed track while retaining high efficiency, (4) electron rejection cut, (5) off-acceptance events rejection cut, (6) requirement of track consistency with TASC energy deposits, and (7) shower development requirement in the IMC. Some of the above selections are described in more detail in the following.

Consistency between MC and flight data (FD) for triggered events is obtained by an offline trigger, which requires more severe conditions than the onboard trigger. It removes non-negligible effects due to positional and temporal variation of the detector gain, and it is applied as a first step of preselection.

In order to reject electronlike events, a "Moliere concentration" along the track in the IMC is calculated by summing up all energy deposits found inside one Moliere radius for Tungsten (± 9 fibers, i.e., 9 mm) around the fiber matched with the track, and normalized to the total energy deposit sum in the IMC. By requiring this quantity to be less than 0.7, most of electrons are rejected while retaining an efficiency above 92% for protons.

Because of the nature of hadronic interaction and combinatorial track reconstruction, there is a possibility to introduce a misreconstruction by erroneously identifying one of the secondary tracks as the primary track. To minimize the fraction of misidentified events, two topological cuts are applied using TASC energy-deposit information irrespective of IMC tracking.

Further rejection is achieved with a consistency cut between the track impact point and center of gravity of energy deposits in the first (TASC-X1) and second (TASC-Y1) layers of the TASC. Energy dependent thresholds are defined using MC simulation to have a constant efficiency of 95% for events that interacted in the IMC below the fourth layer, which are suitable for determining charge, energy, and trigger efficiency (hereafter denoted as "target" events).

Backscattered particles produced in the shower affect both the trigger and the charge determination. Primary particles below the trigger thresholds might be triggered anyway because of backscattered particles hitting TASC-X1 and IMC bottom layers. Moreover the large amount of shower particle tracks backscattered from TASC may induce fake charge identification by releasing additional amounts of energy that add up to the primary particle ionization signal, resulting in a shift of the charge distribution and a larger width.

Since a fraction of events triggered by backscattering is not reproduced well by the simulations, rejection of such events is important. For this purpose, the energy deposit sum along the shower axis over ± 9 fibers (in total 19 fibers) is used to ensure the existence of a shower core in the IMC. This definition differs from the one used for electrons considering the wider lateral spread of hadronic showers. In order to fully exploit the rejection capability of events triggered by backscattering, it is important to set an appropriate threshold as a function of energy. Energy dependent thresholds are defined to get 99% efficiency for "target" events.

The identification of cosmic-ray nuclei via a measurement of their charge is carried out with two independent subsystems that are routinely used to cross-calibrate each other: the CHD and the IMC [52]. The latter samples the ionization deposits in each layer, thereby providing a multiple dE/dx measurement with a maximum of 16 samples along the track. The interaction point is first reconstructed [53] and only the dE/dx ionization clusters from the layers upstream the interaction point are used. The charge value is evaluated as a truncated mean of the valid samples with a truncation level set at 70%.

To mitigate the backscattering effects, an energy dependent charge correction to restore the nominal peak positions of protons and helium to $Z = 1$ and 2 is applied separately

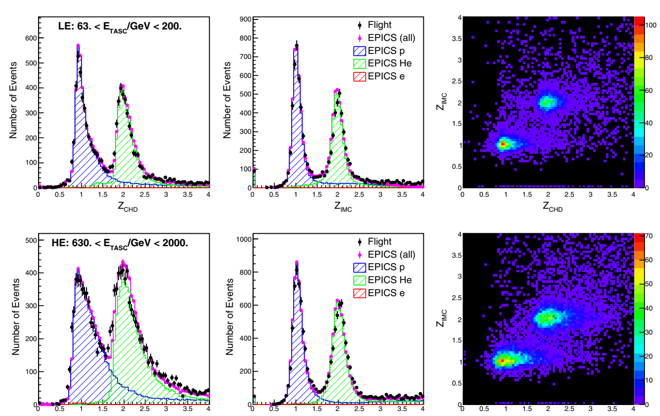

FIG. 2. Examples of CHD/IMC charge distributions. Left, center, and right panels show the CHD charge, IMC charge, and correlation between CHD and IMC charges, respectively. Top and bottom plots correspond to events with $63 < E_{\mathrm{TASC}} < 200$ GeV and $630 < E_{\mathrm{TASC}} < 2000$ GeV, respectively. An enlarged version of the figure is available as Fig. S1 in the Supplemental Material [54].

to FD, EPICS, FLUKA, and GEANT4, where the same correction is used for both protons and helium. Charge selection of proton and helium candidates is performed by applying simultaneous window cuts on CHD and IMC reconstructed charges. The resultant charge distributions are exemplified in Fig. 2. For the selection with the CHD and IMC, energy dependent thresholds are defined separately for the CHD and IMC to keep 95% efficiency for "target" events.

In the lower energy region, the use of the LE trigger is necessary to avoid trigger threshold bias due to the sharp drop in efficiency at $E < 100$ GeV, an effect that extends to the higher energy region via the energy unfolding procedure. With the exception of the offline trigger confirmation threshold which is adjusted to match the hardware trigger, the event selection criteria used in HE and LE analyses are identical. Figure 3 shows the effective acceptance of LE- and HE-trigger analyses after applying all the selection criteria. While the overall difference between the two analyses is rather small, the difference in the low-energy region is sizable.

Background contamination is estimated from the MC simulation of protons, helium, and electrons as a function of observed energy. Among them, the dominant component is off-acceptance protons except for the highest energy region $E_{\mathrm{TASC}} \sim 10$ TeV, where helium contamination becomes dominant. Overall contamination is estimated below a few percent, and at maximum ~5% in the lowest and highest energy region. The correction is carried out before performing the energy unfolding procedure, which is described in the following.

In order to take into account the relatively limited energy resolution (observed energy fraction is around 35% and the resultant energy resolution is 30%–40%), energy unfolding is necessary to correct for bin-to-bin migration effects. In this analysis, we used the Bayesian approach implemented in the ROOUNFOLD package [55,56] in ROOT [57], with the response matrix derived using MC simulation. Convergence is obtained within two iterations, given the relatively accurate prior distribution obtained from the previous observations, i.e., AMS-02 [6] and CREAM-III [8].

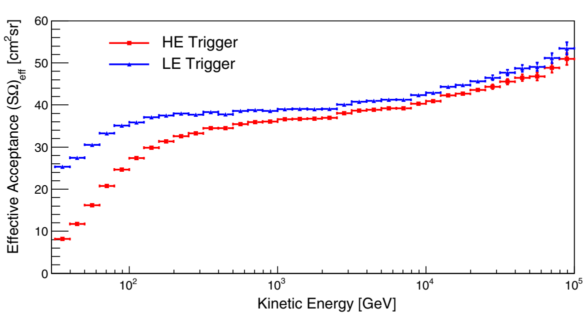

FIG. 3. Comparison of effective acceptance for HE-trigger (red) and LE-trigger (blue) analyses, obtained by MC simulation. The difference between the two selections is the offline trigger confirmation only.

The proton spectrum is obtained by correcting the effective geometrical acceptance with the unfolded energy distribution as follows:

$$\Phi(E) = \frac{n(E)}{(S\Omega)_{\mathrm{eff}}(E)T\Delta E},$$
$$n(E) = U\left(n_{\mathrm{obs}}(E_{\mathrm{TASC}}) - n_{\mathrm{bg}}(E_{\mathrm{TASC}})\right),$$

where ΔE denotes the energy bin width, $U()$ the unfolding procedure based on Bayes theorem, $n(E)$ the bin counts of the unfolded distribution, $n_{\mathrm{obs}}(E_{\mathrm{TASC}})$ those of observed energy distribution (including background), $n_{\mathrm{bg}}(E_{\mathrm{TASC}})$ the bin counts of background events in the observed energy distribution, $(S\Omega)_{\mathrm{eff}}$ the effective acceptance including all selection efficiencies, and T the live time.

Depending on the on-orbit trigger mode and corresponding offline-trigger threshold, two spectra are obtained with the LE and HE analyses, respectively, as shown in Fig. S2 in the Supplemental Material [54]. For $E < 200$ GeV, the use of LE-trigger analysis is required because an offline trigger threshold higher than in the hardware trigger was found to introduce an efficiency bias in the HE-trigger analysis, which became evident with a scan of the offline-trigger threshold using LE-trigger data. Since both fluxes are well consistent in $E > 200$ GeV, they are combined around $E \sim 300$ GeV, taking into account the different statistics of the two trigger modes.

Systematic uncertainties.—Dominant sources of systematic uncertainties in proton analysis include (1) hadronic interaction modeling, (2) energy response, (3) track reconstruction, and (4) charge identification. To address these uncertainties, various approaches are used as discussed in the Supplemental Material [54]. An important part of systematics comes from the accuracy of the beam test calibration and its extrapolation or interpolation. The stability of the measured spectrum against variations of several analysis cuts is also a crucial tool to estimate the associated uncertainties.

Considering all of the above contributions, the total systematic uncertainty, as summarized in Fig. S4 in the Supplemental Material [54], is within 10% and estimated separately for normalization and energy dependent uncertainties.

Results.—Figure 4 shows the proton spectrum measured with CALET in an energy range from 50 GeV to 10 TeV, where current uncertainties that include statistical and systematic errors are bounded within a gray band. The measured proton flux and the statistical and systematic errors are tabulated in Table I of the Supplemental Material [54]. In Fig. 4, the CALET spectrum is compared with recent experiments from space (PAMELA [58,59], AMS-02 [6], and NUCLEON [34]) and from the high altitude balloon experiments (BESS-TeV [60], ATIC-2 [1], CREAM-I [4], and CREAM-III [8]). Our spectrum is in good agreement with the very accurate magnetic

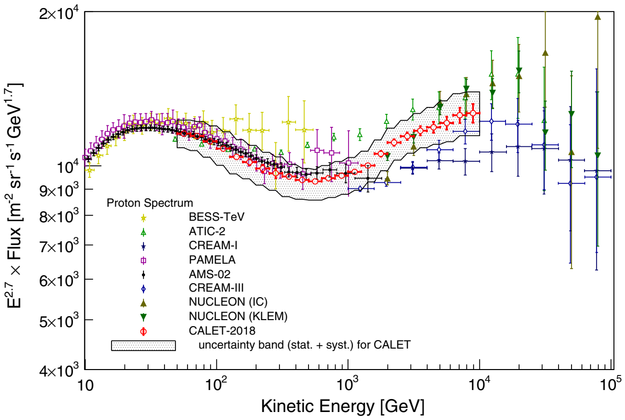

FIG. 4. Cosmic-ray proton spectrum measured by CALET (red points) from 50 GeV to 10 TeV. The gray band indicates the quadratic sum of statistical and systematic errors. Also plotted are recent direct measurements [1,4,6,8,34,58–60]. An enlarged version of the figure is available as Fig. S6 in the Supplemental Material [54].

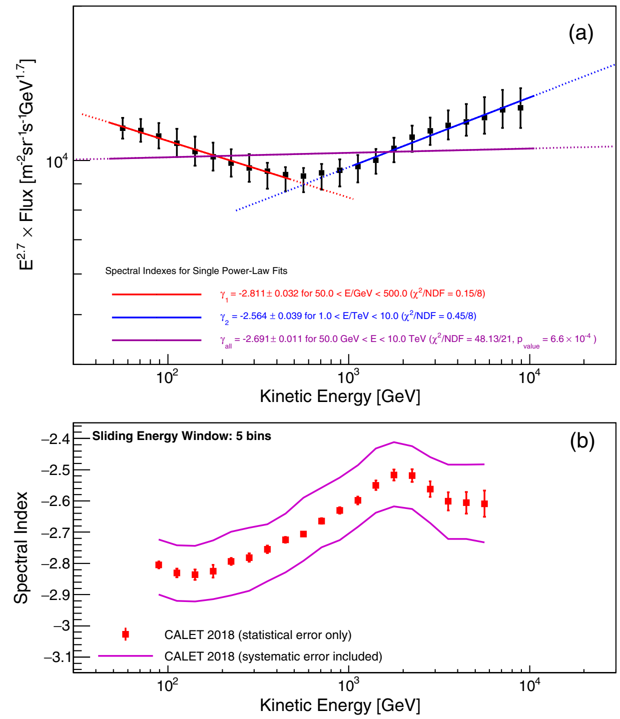

FIG. 5. (a) Fit of the CALET proton spectrum with single power-law functions. Red, blue, and magenta lines indicate the fit result for the energy ranges between 50 and 500 GeV, 1 and 10 TeV, and 50 GeV and 10 TeV, respectively. (b) Energy dependence of the spectral index calculated within a sliding energy window for CALET (red squares). The spectral index is determined for each bin by fitting the data using ±2 energy bins. Magenta curves indicate the uncertainty range including systematic errors.

spectrometer measurements by AMS-02 in the low-energy region, and the spectral behavior is also consistent with measurements from calorimetric instruments in the higher energy region.

Figure 5(a) shows the fits of the CALET proton spectrum with a single power law. In order to study the spectral behavior, only the energy dependent systematics are included in the data points. Red, blue, and magenta lines indicate the fit result for the energy intervals between 50 and 500 GeV, 1 and 10 TeV, and 50 GeV and 10 TeV, respectively. The fit yields $\gamma_1 = -2.81 \pm 0.03$ at lower energy (neglecting solar modulation effects) and $\gamma_2 = -2.56 \pm 0.04$ at higher energy with good chi-square values. On the other hand, the whole range fit gives a large chi-square per degree of freedom, disfavoring the single power-law hypothesis by more than 3σ. Our spectrum can also be fitted with a smoothly broken power-law function [6,61] as shown in Fig. S7 of the Supplemental Material [54], resulting in a power-law index of -2.87 ± 0.06 (including solar modulation effects) below the breakpoint rigidity, which is in good agreement with AMS-02 [6]. A larger variation of the power-law index of 0.30 ± 0.08 and a higher breakpoint rigidity of 496 ± 175 GV than AMS-02 [6] are observed, though the latter is affected by relatively large error.

Furthermore, Fig. 5(b) shows the energy dependence of the spectral index calculated within a sliding energy window (red squares). The spectral index is determined for each bin by a fit of the data including the neighbor ±2 bins. Magenta curves indicate the uncertainty band including systematic errors. This result confirms a clear hardening of the spectrum above a few hundred GeV. These results may be important for the interpretation of the proton spectrum (e.g., [17,18,31]), since they indicate a progressive hardening up to the TeV region, while in good agreement with magnet spectrometers in the 100 GeV to sub-TeV region.

Conclusion.—We have measured, for the first time with an experimental apparatus in low Earth orbit, the cosmic-ray proton spectrum from 50 GeV to 10 TeV, covering with a single instrument the whole energy range previously investigated by magnetic spectrometers (BESS-TEV, PAMELA, and AMS-02) and calorimetric instruments (ATIC, CREAM, and NUCLEON) covering, in most of the cases, separate subranges of the region explored so far by CALET. Our observations confirm the presence of a spectral hardening above a few hundred GeV. Our spectrum is not consistent with a single power law covering the whole range, while both 50–500 GeV and 1–10 TeV subranges can be separately fitted with single power-law functions, with the spectral index of the lower (higher) energy region being consistent with AMS-02 [6] (CREAM-III [8]) within errors. With the observation of a smoothly broken power law and of an energy dependence of the spectral index, CALET's proton spectrum will contribute to shed light on the origin of the spectral hardening. Improved statistics and better understanding of the instrument based on the analysis of additional flight data during the ongoing five years (or more) of observations might reveal a charge dependent energy cutoff possibly due to the acceleration limit in supernova remnants in proton and helium spectra, or set important constraints on the acceleration models.

We gratefully acknowledge JAXA's contributions to the development of CALET and to the operations onboard the International Space Station. We also express our sincere gratitude to ASI and NASA for their support of the CALET project. This work was supported in part by JSPS Grant-in-Aid for Scientific Research (S) Grant No. 26220708, JSPS Grant-in-Aid for Scientific Research (B) Grant No. 17H02901, and by the MEXT-Supported Program for the Strategic Research Foundation at Private Universities (Grant No. S1101021) at Waseda University. The CALET effort in the United States is supported by NASA through Grants No. NNX16AB99G, No. NNX16AC02G, and No. NNH14ZDA001N-APRA-0075.

*yoichi.asaoka@aoni.waseda.jp
†piersimone.marrocchesi@pi.infn.it
‡torii.shoji@waseda.jp

[1] A. Panov *et al.*, Bull. Russ. Acad. Sci. Phys. **71**, 494 (2007).
[2] H. Ahn *et al.*, Astrophys. J. **707**, 593 (2009).
[3] H. Ahn *et al.*, Astrophys. J. Lett. **714**, L89 (2010).
[4] Y. Yoon *et al.*, Astrophys. J. **728**, 122 (2011).
[5] O. Adriani *et al.*, Science **332**, 69 (2011).
[6] M. Aguilar *et al.* (AMS Collaboration), Phys. Rev. Lett. **114**, 171103 (2015).
[7] M. Aguilar *et al.* (AMS Collaboration), Phys. Rev. Lett. **115**, 211101 (2015).
[8] Y. Yoon *et al.*, Astrophys. J. **839**, 5 (2017).
[9] M. Aguilar *et al.* (AMS Collaboration), Phys. Rev. Lett. **119**, 251101 (2017).
[10] M. Aguilar *et al.* (AMS Collaboration), Phys. Rev. Lett. **120**, 021101 (2018).
[11] M. Aguilar *et al.* (AMS Collaboration), Phys. Rev. Lett. **121**, 051103 (2018).
[12] D. Ellison, L. Drury, and J.-P. Meyer, Astrophys. J. **487**, 197 (1997).
[13] M. A. Malkov, P. H. Diamond, and R. Z. Sagdeev, Phys. Rev. Lett. **108**, 081104 (2012).
[14] A. Erlykin and A. Wolfendale, Astropart. Phys. **35**, 449 (2012).
[15] S. Thoudam and J. R. Hörandel, Mon. Not. R. Astron. Soc. **421**, 1209 (2012).
[16] G. Bernard, T. Delahaye, Y.-Y. Keum, W. Liu, P. Salati, and R. Taillet, Astron. Astrophys. **555**, A48 (2013).
[17] P. Blasi, E. Amato, and P. D. Serpico, Phys. Rev. Lett. **109**, 061101 (2012).
[18] R. Aloisio and P. Blasi, J. Cosmol. Astropart. Phys. 07 (2013) 001.
[19] V. Ptuskin, V. Zirakashvili, and E. Seo, in *Proceedings of the 32nd ICRC*, Vol. 6 (Institute of High Energy Physics, Beijing, China, 2011), p. 240.
[20] S. Thoudam and J. Hörandel, Astron. Astrophys. **567**, A33 (2014).
[21] L. Drury, Mon. Not. R. Astron. Soc. **415**, 1807 (2011).
[22] Y. Ohira and K. Ioka, Astrophys. J. Lett. **729**, L13 (2011).
[23] Y. Ohira, N. Kawanaka, and K. Ioka, Phys. Rev. D **93**, 083001 (2016).
[24] P. Biermann, J. K. Becker, J. Dreyer, A. Meli, E.-S. Seo, and T. Stanev, Astrophys. J. **725**, 184 (2010).
[25] V. Ptuskin, V. Zirakashvili, and E. Seo, Astrophys. J. **763**, 47 (2013).
[26] V. Zatsepin and N. Sokolskaya, Astron. Astrophys. **458**, 1 (2006).
[27] N. Tomassetti, Astrophys. J. Lett. **752**, L13 (2012).
[28] A. Vladimirov, G. Jóhannesson, I. Moskalenko, and T. Porter, Astrophys. J. **752**, 68 (2012).
[29] N. Tomassetti, Phys. Rev. D **92**, 063001 (2015).
[30] G. Giacinti, M. Kachelrieß, and D. Semikoz, J. Cosmol. Astropart. Phys. 07 (2018) 051.
[31] C. Evoli, P. Blasi, G. Morlino, and R. Aloisio, Phys. Rev. Lett. **121**, 021102 (2018).
[32] N. Kawanaka and S. Yanagita, Phys. Rev. Lett. **120**, 041103 (2018).
[33] E. Atkin *et al.*, J. Cosmol. Astropart. Phys. 07 (2017) 020.
[34] E. Atkin *et al.*, JETP Lett. **108**, 5 (2018).
[35] S. Torii *et al.* (CALET Collaboration), in *Proceeding of Science (ICRC2017)* (SISSA, Busan, Korea, 2017), p. 1092.
[36] Y. Asaoka, Y. Ozawa, S. Torii *et al.* (CALET Collaboration), Astropart. Phys. **100**, 29 (2018).
[37] O. Adriani *et al.* (CALET Collaboration), Phys. Rev. Lett. **119**, 181101 (2017).
[38] O. Adriani *et al.* (CALET Collaboration), Phys. Rev. Lett. **120**, 261102 (2018).
[39] Y. Asaoka, Y. Akaike, Y. Komiya, R. Miyata, S. Torii *et al.* (CALET Collaboration), Astropart. Phys. **91**, 1 (2017).
[40] P. Maestro, N. Mori *et al.* (CALET Collaboration), in *Proceedings of Science (ICRC2017)* (SISSA, Busan, Korea, 2017), p. 208.
[41] K. Kasahara, in *Proceedings of 24th International Cosmic Ray Conference, Rome, Italy*, edited by N. Iucci and E. Lamanna (International Union of Pure and Applied Physics, 1995) Vol. 1, p. 399, http://adsabs.harvard.edu/full/1995ICRC....1..399K.
[42] EPICS and COSMOS versions are 9.20 and 8.00, respectively.
[43] Y. Akaike *et al.* (CALET Collaboration), in Proceedings of 33rd International Cosmic Ray Conference (ICRC2013) (Brazilian Journal of Physics, Rio de Janeiro, Brazil, 2013), p. 726.
[44] T. Niita, S. Torii, Y. Akaike, Y. Asaoka, K. Kasahara, S. Ozawa, and T. Tamura, Adv. Space Res. **55**, 2500 (2015).
[45] Y. Akaike *et al.* (CALET Collaboration), in *Proceeding of Sciences (ICRC2015)* (SISSA, Hague, Netherlands, 2015), p. 613.
[46] T. Tamura *et al.* (to be published).
[47] T. Böhlen, Nucl. Data Sheets **120**, 211 (2014).
[48] A. Ferrari, P. Sala, A. Fassó, and J. Ranft, CERN, Reports No. INFN/TC_05/11, No. SLAC-R-773, No. CERN-2005-10, 2005.
[49] The version of FLUKA is FLUKA2011.2c.4.
[50] S. Agostinelli *et al.*, Nucl. Instrum. Methods Phys. Res., Sect. A **506**, 250 (2003).

[51] GEANT4 version employs FTFP_BERT as a physics list which is recommended for the simulation of high energy showers.
[52] P. S. Marrocchesi *et al.* (CALET Collaboration), in *Proceeding of Science (ICRC2017)* (SISSA, Busan, Korea, 2017), p. 156.
[53] P. Brogi *et al.* (CALET Collaboration), in *Proceedings of Science (ICRC2015)* (SISSA, Hague, Netherlands, 2015), p. 585.
[54] See the Supplemental Material at http://link.aps.org/supplemental/10.1103/PhysRevLett.122.181102 for supporting figures and the tabulated proton fluxes, as well as the description of data analysis procedure and the detailed assessment of systematic uncertainties.
[55] T. Adye, arXiv:1105.1160v1.
[56] G. D'Agostini, Nucl. Instrum. Methods Phys. Res., Sect. A **362**, 487 (1995).
[57] R. Brun and F. Rademakers, Nucl. Instrum. Methods Phys. Res., Sect. A **389**, 81 (1997).
[58] O. Adriani *et al.*, Phys. Rep. **544**, 323 (2014).
[59] O. Adriani *et al.*, Riv. Nuovo Cimento **40**, 1 (2017).
[60] S. Haino *et al.*, Phys. Lett. B **594**, 35 (2004).
[61] L. Glesson and W. Axford, Astrophys. J. **154**, 1011 (1968).